E-WEHP: A Batteryless Embedded Sensor-Platform Wirelessly Powered From Ambient Digital-TV Signals

Rushi J. Vyas, *Member, IEEE*, Benjamin B. Cook, Yoshihiro Kawahara, *Member, IEEE*, and Manos M. Tentzeris, *Fellow, IEEE*

***Abstract*—The use of digital television broadcasting standards has resulted in transmission of perpetually on wireless digital-TV signals over the air at wider bandwidths in ultrahigh-frequency bands for high-definition video and audio broadcasts to TV and smart phones. This paper presents a unique embedded wireless energy-harvesting prototype (E-WEHP) that exploits the unique makeup of ambient digital-TV signals, and scavenges wireless power from them at distance of over 6.3 km from the TV broadcast source. The harvested wireless power is successfully used to power and sustain a 16-bit embedded microcontroller for sensing and machine-to-machine applications without the use of batteries. The E-WEHP uses a miniaturized planar log-periodic antenna and RF-dc charge-pump circuit with maximum sensitivities of −14.6 and −18.86 dBm and an embedded firmware-based power management scheme to power microcontroller peripherals from different types of ambient digital-TV signals.**

***Index Terms*—Antenna, autonomous sensors, charge-pump, digital TV, embedded microcontroller, energy harvesting, power scavenging, RF-dc, ultrahigh-frequency (UHF), voltage multiplier, wireless power.**

I. Introduction

THE ADVENT of digital broadcasting standards for transmission of TV signals over the air (ATSC, DVB-T, and ISDB-T) since the 1990s has resulted in huge payloads of data being broadcasted wirelessly at ultrahigh-frequency (UHF) bands. Rather than carry video signals over a single frequency, audio and video streams are sent at digitally modulated closely spaced carrier orthogonal frequency-division multiplexing (COFDM) frequencies referred to as orthogonal frequency-division multiplexing (OFDM), which allows for transmission of a much more enhanced picture quality without suffering ghosting and multi-path effects prevalent with analog TV. Digital TV broadcasts have lower transmit power compared to older analog TV, and are designed to beam out high-definition TV (HDTV) programs for long duration of time and wider coverage in most urban areas. Ambient wireless power in the UHF bands due to digital-TV broadcasts can offer a perpetual power source for sustaining batteryless limited duty-cycle operations of a number of low-power (LP) embedded and wireless transceivers.

In this paper, we present a unique embedded wireless energy-harvesting prototype (E-WEHP) capable of scavenging wireless power from digital-TV broadcasts over range of several kilometers for powering on LP embedded processors and wireless transceivers [1]. The primary application of the E-WEHP is a pervasive way to power on embedded sensors deployed over a large geographic area using ambient wireless digital-TV signals present in the air without using batteries. Through the proper design and integration of an RF front-end and embedded software, ambient wireless power has been successfully harvested and stored in low-leakage capacitors to sustain a 16-bit microcontroller for sensing operations 6.3 km from a wireless TV broadcast source. The use of low-leakage capacitors to collect and use ambient wireless signals as a power source offers substantial benefits over batteries. Capacitors are capable of higher number of charge–discharge cycles at low equivalent series resistance (ESR), thereby enabling them to source or sink higher amounts of charge unlike lithium-ion batteries. Capacitors do not degrade with shallow discharge like NiCADs, and are not volatile when exposed to moisture or harsh handling like lithium-ion batteries. Capacitors are also much more environmentally friendly since they do not use heavy metals and have no disposal issues. The logistical benefit of eliminating periodic battery replacement makes the E-WEHP ideal for applications such as structural-health monitoring, monitoring radio-isotope levels in the air, environmental and agricultural sensing, and for "Internet of Things."

II. Related Work

Wireless power transfer mechanisms are primarily classified as near- or far-field systems. Near-field systems use magnetic induction to transfer power wirelessly with high efficiency typically within a wavelength from the source. However, beyond near-field, magnetic fields decay rapidly at a rate of 60 dB/decade, which make them useful only for distances

Manuscript received October 26, 2012; revised March 21, 2013; accepted March 26, 2013. Date of publication May 03, 2013; date of current version May 31, 2013. This work was supported by the U.S. National Science Foundation (NSF) and the New Energy and Industrial Technology Development Organization of Japan (NEDO). This work is an expanded version of the paper presented at the IEEE MTT-S International Microwave Symposium, Montreal, QC, Canada, June 19, 2012.

R. J. Vyas, B. B. Cook, and M. M. Tentzeris are with the ATHENA Research Group, Georgia Institute of Technology, Atlanta, GA 30332 USA (e-mail: Rushi.Vyas@gatech.edu; bcook40@mail.gatech.edu; etentze@ece.gatech.edu).

Y. Kawahara is with the ATHENA Research Group, Georgia Institute of Technology, Atlanta, GA 30332 USA, and also with the Department of Information and Communication Engineering, University of Tokyo, Tokyo 113-8656, Japan (e-mail: kawahara@akg.t.u-tokyo.ac.jp).

Color versions of one or more of the figures in this paper are available online at http://ieeexplore.ieee.org.

Digital Object Identifier 10.1109/TMTT.2013.2258168

TABLE I
ENERGY HARVESTING COMPARISONS [19], [21], [39]

Project	RF Sensitivity/ DC output	RF Source	Load	Range/ Rx Antenna Gain	Process
Karalis [8]	NA	9.9 MHz, 60W near-field	Light bulb	2m	Coil
NXP UCode [44]	-12.6dBm single tone	RFID reader: 4W EIRP, 900MHz	Control logic, SRAM	-	CMOS
Karthaus [18]	-17.8dBm @ 1.5V, 1.5μA single tone	RFID reader: 4W EIRP, 900MHz	Control Logic, EEPROM	9.25m, -0.5dBi	0.5 μm CMOS
Reinisch [15]	-19.7dBm @ 1.1V, 158nA single tone	RFID reader: 4W EIRP, 900MHz	Temp sensor, Tx	-	0.13 μm CMOS
Yin [16]	-6dBm @ 1V, 2.4μW single tone	RFID reader: 4W EIRP, 900MHz	Temp Sensor	-	0.18 μm CMOS
Yeager [17]	-12 dBm @ 9μA	RFID reader: 4W, 900MHz	Temp Sensor	3m	0.13 μm CMOS & PCB
Power Cast P2110 [19]	-11.5dBm @ 1.2V	Transmitter 915 MHz	Battery	8m, 6dBi	CMOS
Dolgov [21]	-15.2 dBm @ 3V with battery-assisted MPPT	Ambient Cellular 1.96 GHz	Battery	50m	PCB
WISP [39]	-9.5dBm @1.9V, 0.7μA	RFID reader: 4W, 900MHz	TI MSP 430F1232 MCU	Theoretical 4.3m, 2dBi	PCB
WISP [22]	NA @ 0.7V, 87.5 μA	Ambient TV Signal 960kW ERP	Temp Sensor	4.1km, 5dBi	PCB
E-WEHP (this work)	-14.6dBm Single tone or -37dBm multi-tone over 2 TV channels @ 1.8V, 1.8 μA	Ambient Digital TV 512-566 MHz, 48kW ERP	16-bit PIC MCU	6.3km, 7.3 dBi	PCB

that are close to the radius of near-field coil-type antennas [2]. Earliest known work on near-field wireless power-transfer was carried out by Tesla in 1891. Tesla's experiment illuminated a light-bulb through near-field magnetic induction at frequencies up to tens of kilohertz [3]. Near-field or inductive wireless-power-transfer (WPT) schemes are also actively being investigated for powering locomotives with powering range of 20 cm or less [4]–[7]. The maximum near-field range that has been achieved is 2 m with 40% efficiency by using a magnetic-resonant power-transferring coil/antenna as reported by Karalis *et al.* [8].

Compared to near-field systems, wireless power in the far-field propagates using transverse electromagnetic waves, which decay less rapidly at about 20 dB/decade, thereby allowing for power transfer over longer range [2]. Bose first demonstrated the use of wireless signals to transfer power and audio signals in the far-field through his invention of the crystal radio in 1894, which is the precursor to the modern AM radio [9]. Since then, a number of RF/wireless energy harvesting work has been reported in frequency bands from 60 Hz to 8 GHz [10], [11]. The biggest use of wireless power has been in RF identifications (RFIDs) for consumer and industrial tracking applications. A number of research groups have also used near- and far-field WPT schemes based on RFID technologies for powering or activating bio-implanted sensors in human body for electrocardiogram (ECG), electroencephalography (EEG), electromyography (EMG), and ocular sensing [12]–[14].

Most of the wireless power harvesting work in the far field has been in the UHF bands between 862–928 MHz for RFID-based sensors, as shown in Table I. Most of the new designs use sub-micron CMOS technology with RF input sensitivities down in the tens of microwatts with a reported range of 9.25 m [15]–[19]. Most of the RFID-based wireless power-harvesting designs are optimized for high sensitivities at a single tone within the RFID operating bands between 862–928 MHz. This is primarily because RFIDs operate only within a range of a conventional RFID reader that emits between 2–4-W effective isotropic radiated power (EIRP) using a frequency-hopping spread spectrum (FHSS) for power and communication. In the FHSS spectrum used in RFIDs, the wireless power is focused within a single 250- or 500-kHz frequency channel that hops between 862–928 MHz in a pseudorandom fashion with a dwell time of 0.4 s [2], [20].

FHSS is well suited for remotely reading 64- or 256-bit data payloads from multiple RF identification (RFID) tags without eavesdropping and collision. It therefore makes sense for RFID tags to maximize RF sensitivity at a single tone within an RFID reader's operating band since it allows for higher range and less collision. Antennas for RFID tags also, for the most part, tend to use an inductive loop to be matched to the capacitive impedance of the RFID chip to increase the rage over which the tag can be powered by an RFID reader. However, high sensitivity at single tones in RFID tags are not suitable for harvesting wireless power from ambient communication signals since most modern communication standards that transmit higher data payloads do not use FHSS-based communication from a dedicated and directive 4-W RFID reader.

In [21], Dolgov *et al.* propose a full-wave rectifier along with a dc to dc boost converter topology to harvest power from ambient cellular signals 50 m from a cellular base station. The harvested power is used to charge a 3-V lithium battery. For stepping up dc voltages, dc to dc converters offer the best efficiency in its class, especially at high input power levels that would be present at closer distances to any wireless power source. However, its efficiency decreases at input power levels below 30 mW [21] that are present further away from the RF power source.

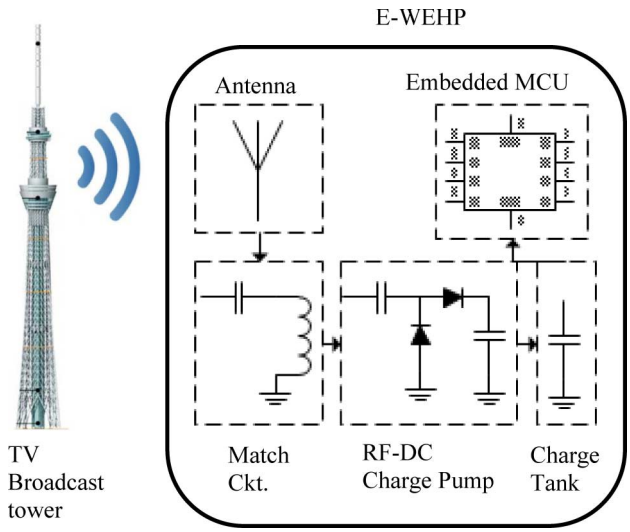

Fig. 1. Wireless energy harvesting prototype system (E-WEHP).

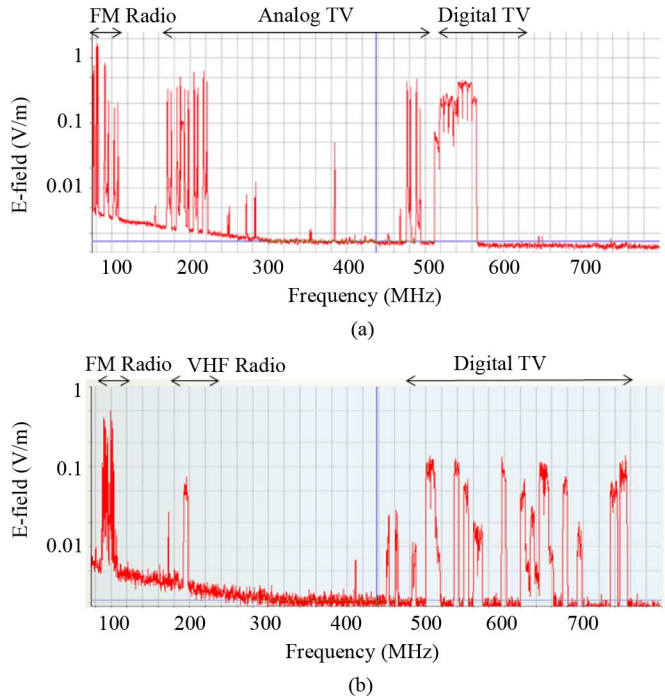

Fig. 2. (a) Ambient wireless radiation measured in downtown Tokyo, Japan. (b) Ambient wireless radiation measured in Midtown Atlanta Equipment used: NARDA SRM-3000 radiation meter in isotropic mode.

The drop is primarily because dc to dc boost converters require a steady-voltage pulse-width modulation (PWM) pulse signal to be applied across its gate drives at all times, which is provided by a microcontroller unit operating in the high current-consuming active mode. The extra power consumed by the PWM signal is provided by a battery, which reduces the range over which the power harvested is greater than the power consumed in the step-up dc to dc converter. In [22], Smith and Sample use a WISP-based RFID platform to continuously power on a commercially available RadioShack thermo and hygrometer from TV signals. The RadioShack meter consuming 1.5 V and 25 μA is powered from a 960-kW effective-radiated-power (ERP) TV broadcast source 4.1 km away. Dolgov and Sample demonstrate the potential of powering LP electronics from a high enough wireless broadcast source within terrestrial distances. To make ambient wireless energy harvesting useful for conventional sensing and machine-to-machine (M2M) applications, embedded processors and radios typically running at 1.8 V or higher need to be powered from lower amount of wireless power at even further distances from broadcast sources. Constraints in power and frequency-spectrum allocation in every modern large-area communication standard is intended to increase spectral usage-efficiency, and decrease transmit power levels, and at the same time be capable of handling ever-increasing number of users and data payloads.

This work is the first of its kind that characterizes the spectral makeup of modern wireless digital-TV signals and presents a platform uniquely optimized to harvest energy from it. The optimized platform, shown in Fig. 1, can sustain 1.8-V embedded-microcontroller operations without battery power at range of over 6.3 km from TV broadcast sources. The different sections of the platform that allow for such long-range operation is summarized as follows: the wireless spectrum in a metropolitan area between 50–900 MHz is measured and wireless power present in wireless TV and cellular frequency bands are closely analyzed for pockets with the highest power per bandwidth. Based on the spectral and geographic location of the wireless power source, an optimized, planar, and broadband antenna for easy mounting and conversion of incident wireless radiation into RF signals is presented. An improved RF-dc charge-pump circuit optimized to rectify and step-up lower levels of RF signals present in multi-carrier digital-TV signals for varying output loads, and store the harvested power in a 100-μF multi-layer ceramic-capacitor (MLCC) surface-mount capacitor is presented. Instead of a hardware-based approach that is used in prior work, an energy-efficient embedded software design to regulate the RF-dc output, and sustain operation of a 1.8-V 16-bit PIC24F microcontroller using the harvested ambient wireless power without the use of batteries or a tethered power supply is presented.

III. Ambient Wireless Power

Wireless spectrum measurements between 50–900 MHz were carried out in downtown Tokyo, Japan, and Atlanta, GA, USA, during peak workday hours using a NARDA SRM-3000 radiation meter [23], as shown in Fig. 2(a) and (b), respectively. The radiation meter is configured with an antenna calibrated in isotropic mode to capture average fluctuations of ambient wireless signals along $x-$, $y-$, and z-planes. Measurements show peak radiation levels in the sub-100-MHz range in Atlanta, GA, USA, and Tokyo, Japan, due to FM radio broadcasts. High radiation levels are also observed in the 100–500-MHz range due to analog-TV broadcasts. Significant radiation levels are also observed in the 500–700-MHz bands due to wireless digital-TV broadcasts that have been deployed globally since 2000. Compared to analog-TV and FM radio signals, digital-TV signals use multiple carriers to transmit significantly more amounts of data within the 500–700-MHz frequency bands over the air, resulting in higher power per bandwidth. Wireless radiation in the

UHF bands between 500–700 MHz also have better propagation characteristics while traversing through the air and physical obstacles such as trees and buildings. Also, with free space wavelengths between 42.3–60 cm, the incident electric field radiations at UHF bands can be efficiently captured with antennas with compact form factors compared to antennas designed for FM and AM radio.

Compared to analog TV standards such as the National Television System Committee (NTSC) and phase alternating line system (PAL) digital TV standards broadcast out much higher data payloads through better spectral efficiency. Each analog TV channel used a 6-MHz bandwidth for only one carrier and its subcarrier that is 4 quadrature amplitude modulation (QAM) modulated to transmit 640 by 483 pixels of video. By comparison, digital TV uses the same 6-MHz bandwidth to send out HDTV content with 1920 by 1080 pixels of video [24], [25]. The higher resolution is achieved by digitally compressing and transmitting video and audio data over multiple carriers within the same 6-MHz frequency channel. In Japan and parts of Asia and South America, wireless digital-TV broadcasts use the integrated services digital broadcasting standard (ISDB-T). Under ISDB-T, HDTV channels use 6-MHz wide channels each between frequency bands of 470 and 770 MHz. Each 6-MHz TV frequency channel has 5617 carriers at 0.99206-kHz frequency spacing, each of which carry video and audio data using 64-QAM and quadrature phase-shift keying (QPSK) modulations at data rates of 2–18 Mbit/s. Since 2009–2010, a similar multi-carrier standard known as the Advanced Television Systems Committee standard (ATSC) has been used for wireless digital-TV broadcasts in North America. ATSC uses MPEG-II compression and an n-mode ASK modulation scheme referred to as 8-VSB in the same 6-MHz TV frequency channel to handle HDTV payloads at rates of 1 GB/s [24].

Digital-TV broadcasts also have lower peak transmit powers of 48 kW compared to a peak of 380 kW for analog TV in Tokyo, Japan. However, due to their multi-carrier makeup, digital-TV signals have higher power per channel bandwidth compared to analog TV and other communication standards. Digital TV signals also have higher immunity against environmental effects, such as atmospheric noise, multipath interferences ("ghosting") effects, co-channel analog TV interference, and stray electromagnetic interference coming from motor vehicles and power lines in urban environments [24], [26] .

A site survey showed the source of the wireless TV broadcasts to be nine different analog and digital-TV channels that are transmitted from atop the Tokyo TV tower at geographical coordinates 35°39′31 N, 139°44′44 E, which is 6.3 km away, as shown in the topographical map in Fig. 3. The transmit antennas for the nine digital TV channels broadcast in all directions from 250 m atop the Tokyo TV tower. The transmit frequencies and power levels (PTX) of the nine digital TV broadcasts are summarized in Table II.

IV. E-WEHP

Converting the ambient wireless radiation due to wireless digital-TV signals into usable power requires the proper design and integration of the different components in the E-WEHP platform. The amount of wireless power present at a single

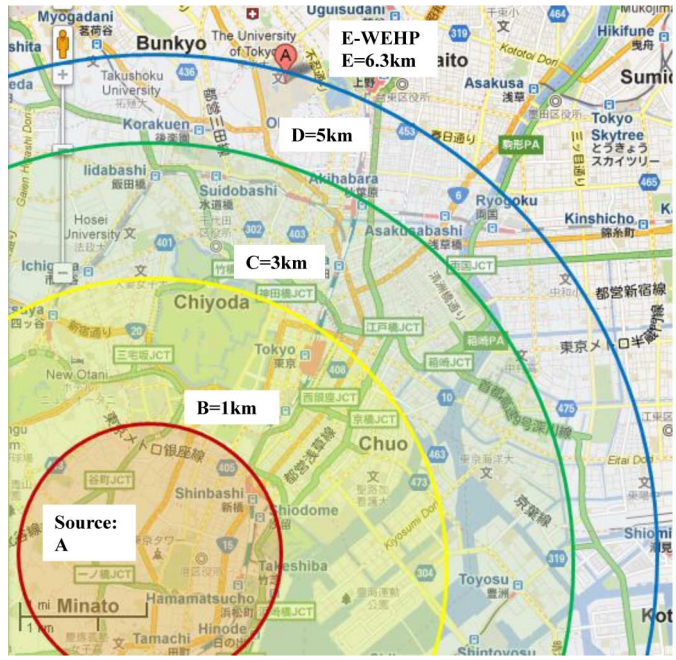

Fig. 3. Location of Tokyo TV broadcast source at A (35°39′31 N 139°44′44 E) with respect to E-WEHP at E (35.712704 N, 139.763277 E) 6.3 km away.

TABLE II
THEORETICAL AND MEASURED SINGLE-CARRIER AND CHANNEL POWER LEVELS USING E-WEHP ANTENNA (GAIN: 5–7.3 dBi)

TV Channel Freq. (MHz)		A P_{TX} Power kW	B 1km μW	C 3km μW	D 5km μW	E 6.3km μW	
						theory	meas
JOMX 512-518	1-tone	5	0.32	0.26	0.21	0.19	0.008
	Channel		37.3	30.3	24.5	22.1	0.93
JO-RX/CX/TX/EX/AX/AB/AK 518-560	1-tone	48	3.6-4.1	2.9-3.4	2.3-2.7	2.2-2.5	0.1-0.25
	Channel		419-478	338-396	268-315	256-291	11.7-29
JOUD 560-566	1-tone	19	1.37	1.08	0.86	0.78	0.032
	Channel		160	126	100	91	3.73

tone or carrier (PCARRIER) at different distances from the TV broadcast source shown in Fig. 3 are determined using the more realistic International Telecommunication Union (ITU) model, as in (1). The ITU model is used since it is found to yield close to accurate results relative to the measurements as compared to other propagation models as per [27]. The received power level is a function of the transmit power broadcasted from the TV tower; the E-WEHP antenna's orientation with respect to the incident field; the E-WEHP's antenna gain (G); the conjugate impedance match between the antenna and the RF to dc converter circuit (S_{11}), which varies with the incident field's frequency (f) and power level, and the output load impedance. In (1), c is the speed of propagation of TV signals in the air; h is the ground clearance of radio propagation; and R is the distance from the TV broadcast source shown in Fig. 3[28].

For digital TV signals, the wireless power is broadcasted not just at one carrier frequency or tone, but at each of the 5617 carriers or tones that make up each of the 6-MHz-wide channels present in the air at all times [25]. The total input power captured ("PCHANNEL") by the E-WEHP is, hence, an aggregate of its response to each of the carriers ($f1$ to fN) that are continuously present in as many TV channels ($c1$ to cN) in the digital TV bands, as in (2)[29]. The carrier and channel power levels at distances of 1, 3, 5, and 6.3 km from the TV tower using the E-WEHP antenna estimated using (1) and (2) are listed in Table II. The E-WEHP antenna used in the estimation and measurements is covered in Section V.

V. E-WEHP Antenna Design

Measurements in Fig. 2 show digital-TV signals as having linear polarization parallel to the ground, and having frequencies between 512–566 MHz. Based on measurements in Fig. 2, a log-periodic antenna is developed for the E-WEHP platform with maximum gain (G) and return-loss (S_{11}) bandwidth based on the relationship in (1) and (2). Based on earlier work done by Isbell and Duhumel from the University of Illinois [30], a well-designed log-periodic antenna has higher gain compared to dipoles and monopoles, and wider bandwidth compared to Yagi antenna arrays. In [31], Carrel presents an empirically derived method of miniaturizing log periodic antennas albeit for a 3-D antenna structure

$$P_{\text{CARRIER}} = P_{\text{TX}} \cdot G \cdot \left(\frac{c}{4\pi \cdot f \cdot R}\right)^2 \cdot \frac{17.3}{2 \cdot h} \cdot \sqrt{\frac{R}{4f}} \cdot (1 - |S_{11}|^2) \quad (1)$$

$$P_{\text{CHANNEL}} = \sum_{c1}^{cN} \int_{f1}^{fN} P_{\text{CARRIER}} \cdot df. \quad (2)$$

For the E-WEHP, a log periodic antenna in 2-D planar form was designed and optimized to capture power from ambient digital TV signals in the air using empirical relationships derived in [31] and [32]. The antenna was designed using CST Microwave Studio to fit on an A-4 sized 0.062-in-thick FR-4 substrate, and have maximum gain and return-loss bandwidth in the 500–600-MHz range where the bulk of the wireless, digital-TV signals are broadcasted as measured in Fig. 2. The planar A-4 form factor allows for unobtrusive placement of the E-WEHP platform on nonmetallic walls and side-rails, while also aligning the antenna's dipole elements parallel to the horizontal electric field of the incident wireless TV signal, thereby minimizing polarization loss.

A six-element log-periodic array with an antenna element scaling factor (τ) of 0.94, a relative element spacing (σ) of 0.18, and dipole lengths ($L_1 - L_6$) of between 24–30 cm is determined to yield maximum gain and bandwidth between 500–600 MHz for an A-4 size array structure. A tooth-like pattern is used to shrink the dipole elements to within A-4 width, while still ensuring that the dipoles have the required effective radiating length ($L_1 - L_6$), as shown in Fig. 4(b). The antenna's impedance was tuned to 50 Ω, and not the capacitive impedance of the diode-capacitor array in the RF-dc charge-pump circuit

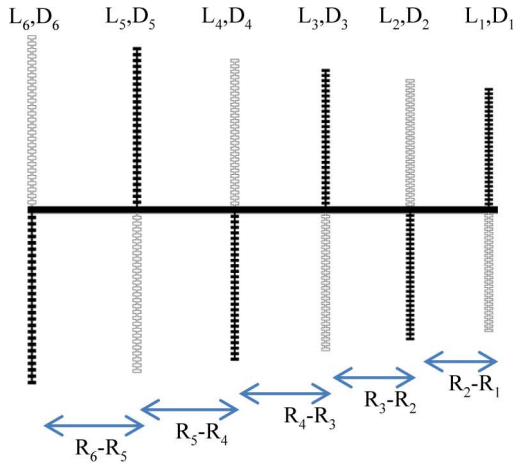

(a)

(b)

Fig. 4. (a) E-WEHP log periodic antenna structure dimensions. (b) E-WEHP log periodic antenna prototype fabricated on 0.062-in FR-4.

since reducing the antenna impedance further also reduced the overall antenna gain [32]. The log periodic antenna was connected to the E-WEHP's RF-dc converter using a standard 3.5-mm SMA cable with its inner conductor and outer shields stripped to feed the dipole elements on the antenna's lower and upper sides, respectively, in the form of an infinite balun, as shown in Fig. 4(b).

The antenna's gain and return loss while placed atop a nonmetallic surface are measured using the Satimo Stargate SG-24 measurement system and Rohde and Schwarz ZVA-8 vector network analyzer, respectively. Simulated and measured antenna gain and return loss are plotted in Figs. 5 and 6, and show good agreement. The antenna has a measured gain of between 5–7.3 dBi and greater than 10-dB return loss

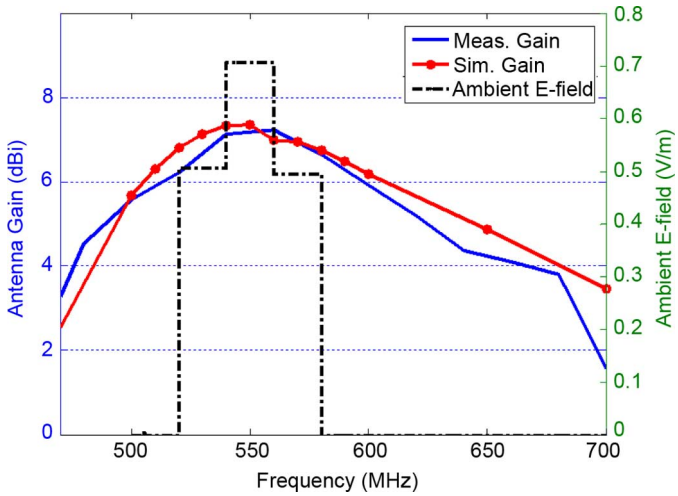

Fig. 5. E-WEHP log periodic antenna simulated and measured gain with respect to ambient wireless radiation due to digital-TV broadcasts in downtown Tokyo, Japan.

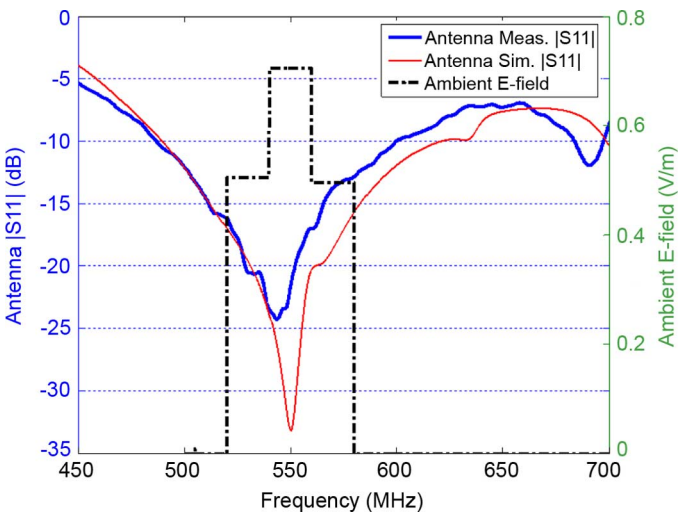

Fig. 6. E-WEHP log periodic antenna simulated and measured return loss with respect to ambient wireless radiation due to digital-TV broadcasts in Tokyo, Japan.

TABLE III
E-WEHP LOG PERIODIC ANTENNA SPECIFICATIONS

	Parameter	Simulated	Measured
Required Specifications	Gain 'G' (dBi)	5-7.4	5-7.3
	Bandwidth 'Bar' (MHz)	500-600	500-600
	Size (cm2)	30 x 21.5	30 x 21.5
Dimensions	Scale Factor 'τ'	0.95	
	Relative Space 'σ'	0.18	
	Angle 'α'	6.59	
	Number of elements 'I'	6	
	L1 (cm) 30		
	L2 (cm) 28.5	R2- R1 (cm)	4.95
	L3 (cm) 27.1	R3- R2 (cm)	5.35
	L4 (cm) 25.75	R4- R3 (cm)	5.65
	L5 (cm) 25.50	R5- R4 (cm)	6.15
	L6 (cm) 24.23	R6- R5 (cm)	6.55

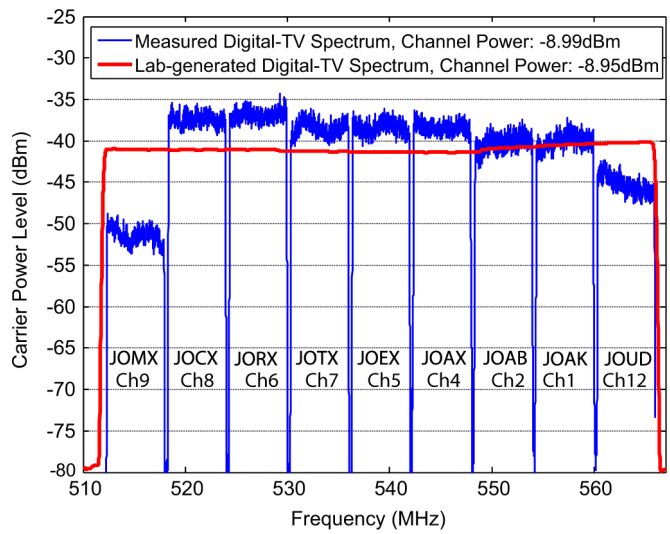

Fig. 7. Wireless power captured by E-WEHP log-periodic antenna from wireless digital-TV signals broadcasted from TV tower 6.3 km away in Tokyo, Japan, showing captured total power of −8.99 dBm (126.2 μW) across nine digital TV channels (blue in online version). Multi-carrier RF signal generated in the laboratory using a Rohde SMJ100A vector signal generator to test E-WEHP (red in online version).

in the 500–600-MHz bands, with peak performance between 540–560 MHz, where peak wireless radiation due to digital TV signals were measured, as shown in Figs. 5 and 6. The antenna array has an end-fire radiation pattern with a half-power beamwidth of 62.7°. The final specifications of the E-WEHP log-periodic antenna are listed in Table III.

The expected carrier and channel power levels received by the E-WEHP antenna at different distances from the TV broadcast are calculated using the ITU model in (1) and (2), respectively, and are listed in Table II. The power received by the E-WEHP log-periodic antenna from the digital-TV signals is measured at location 35.712704 N, 139.763277 E by connecting the antenna to a Tektronics RSA3308B spectrum analyzer, and aligning the antenna toward the Tokyo TV tower 6.3 km away. The response of the antenna to each of the incident digital-TV signals is shown in the spectrum plot of Fig. 7. The carrier and channel power levels received by the antenna from each of the digital-TV channels are listed in Table III.

At 6.3 km away from the TV broadcast source, the peak carrier power level captured by the antenna is only about −35 dBm (0.32 μW), whereas the total channel power captured from the combined nine channels aggregate up to −8.99 dBm (126.2 μW). The channel power received by the antenna from each channel varies from between −15.57 dBm (27.7 μW) for TV channel #6 (JORX TV: 524-530 MHz), and approximately −30 to −27 dBm (1.8 μW) for TV channel #9 (JOMX: 512-518 MHz). The measured power captured by the antenna 6.3 km from the source is found to be lower than the ITU model. The higher ITU estimate is because the radius of the first Fresnel zone used in the path-loss computation is taken as the distance between the line of propagation and the ground. The actual terrain, however, contained

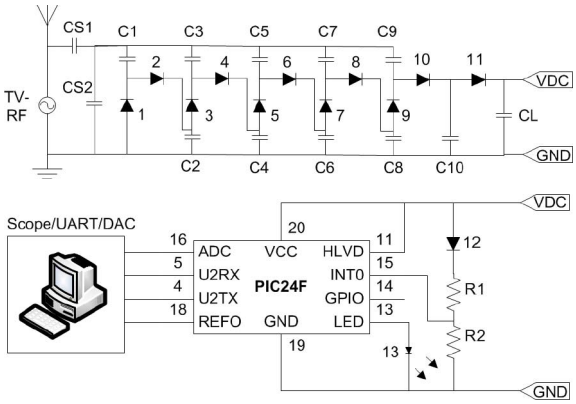

Fig. 8. E-WEHP system schematic.

buildings whose heights were not available for more accurate estimation of the Fresnel-zone radius for ITU estimation.

VI. RF Charge-Pump Design

A. Design and Simulation

The E-WEHP platform was fitted with an ultra-LP RF-dc charge-pump circuit that is customized to step up, rectify, and collect power from the sub-microwatt carrier signals across multiple carriers present in several TV channels that the E-WEHP log-periodic antenna receives. Using just the LP levels present at terrestrial distances from the source shown in Fig. 3, the RF-dc charge-pump circuit is designed to produce output voltages of larger than 1.8 V across an output load. The output load comprises of a 100-μF low-leakage MLCC capacitor in parallel with a varying load that is produced by a PIC24F microcontroller operating in different modes required for sensing applications.

For LP multi-carrier signals shown in Fig. 7, the RF-dc charge-pump circuit has a varying response with respect to frequency, input power levels, and the output load. In [33], Vita and Iannaccone theoretically prove that for single-tone input power levels in the 20-80-mW range, RF-dc charge-pumps containing between 3–5 stages yield the maximum output voltage for the least amount of input power. A five-stage RF-dc charge-pump circuit is designed and optimized using the Agilent Advanced Design System (ADS) RF system simulator using the harmonic-balance method in the 500–600-Hz frequency range. Transient analysis are more useful at estimating the RF-dc's input impedance with respect to power levels and output load, but require step-time resolution of nanoseconds and end time in minutes due to the 100-μF output load. Hence, computer memory size constraints limit the use of transient analysis with RF-dc charge-pump circuits.

In Fig. 8, during each consecutive negative half-cycle of the input RF ac signal, capacitors C1, C3, C5, C7, and C9 get charged to a voltage equal to the input RF voltage plus the voltage across the preceding even numbered capacitor through diodes D1, 3, 5, and 7, respectively, minus the forward voltage loss across each diode. During the positive half cycle of the RF input signal, the even-numbered capacitors get charged in a similar fashion through forward-biased diodes D2, 4, 6, 8, and 10 with opposite polarities shown in Fig. 8. The voltage across

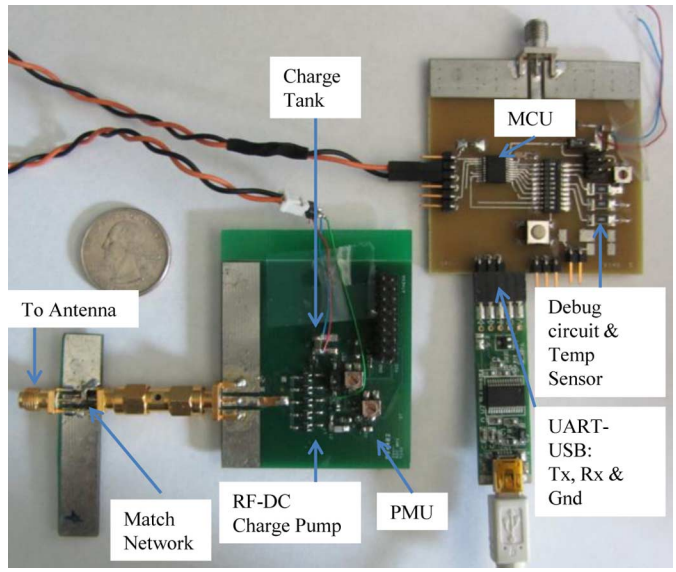

Fig. 9. E-WEHP RF to dc charge-pump circuit prototype.

the output charge-tank capacitor as a function of a single tone of the input RF voltage induced across the antenna is estimated by (3), where x is the number of charge-pump stages, and V_f is the voltage induced at the input due to each carrier present in the digital-TV signal. The output voltage of the RF-dc charge-pump is adversely affected by the forward voltage drop across the diode junction (V_d) due to which low-barrier Schottky diodes with the lowest available forward voltage and junction capacitance at microampere current levels were used. Circuit traces were kept as small as possible to minimize substrate losses. The RF-dc charge-pump prototype was fabricated on standard 0.062-in FR-4 substrate, and is shown in Fig. 9,

$$V_{\mathrm{CAP}} = 2 \cdot x \cdot V_f - (2 \cdot x + 1) \cdot V_d. \tag{3}$$

B. Impedance Model

The overall loss in the RF-dc charge-pump can be gauged from its input impedance that is typically represented as a series *RC* circuit, with *R* representing losses including forward voltage losses of the diodes, and *C* representing the equivalent capacitance of the charge-pump circuit [33]–[35]. During simulation, the circuit parameters, namely, capacitors C_1–C_{10}, are optimized to maximize the voltage output across the charge-tank capacitor for a given input power level, or conversely reduce the series losses in the circuit at frequencies where the ambient TV signals are present. Low-leakage MLCC capacitors with values of 20 and 15 pF were used for all the even- and odd-numbered capacitors, respectively, in Fig. 8. The input resistance of the RF-dc charge-pump circuit was measured using a Rohde and Schwartz ZVA-8 vector network analyzer and show low losses of between 0.5–0.55 Ω, as shown in Fig. 10, and capacitive reactance of between 3–13 Ω at the TV channel frequencies.

The basic single-tone response of the E-WEHP RF-dc charge-pump without any impedance mismatch effects is a good gauge to study its RF-dc response at different frequencies within the digital TV bands. The input single-tone power ($P_{\mathrm{Turn\text{-}on}}$) required at different TV channel frequencies to charge up the

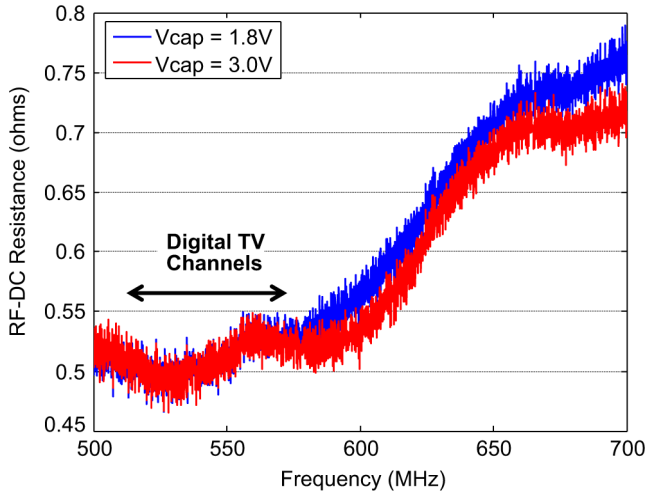

Fig. 10. E-WEHP RF to dc charge-pump circuit input resistance for charge-tank voltages of 1.8 and 3.0 V, respectively.

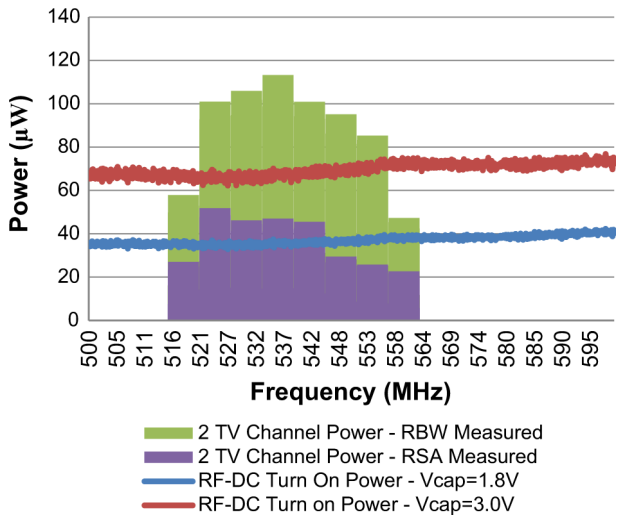

Fig. 11. E-WEHP RF to dc charge-pump circuit input power for charge-tank voltages of 1.8 and 3.0 V, respectively.

charge-tank to 1.8 and 3.3 V is determined using (4) and is plotted in Fig. 11. The single-tone response shows the RF-dc charge-pump needing the least amount of RF input power between 516–564 MHz where most of the TV channels measured in downtown Tokyo, Japan, are present,

$$P_{\text{Turn-on}} = P_{\text{CARRIER}} \cdot (1 - |S_{11}|^2). \tag{4}$$

The mostly capacitive impedance of the RF to dc charge-pump circuit is matched to the 50-Ω impedance of the log-periodic antenna to minimize input return losses (S_{11}), and maximize the power captured by the E-WEHP from the incident digital-TV signals, as in (2). A mixed L-section matching network comprising of lumped discrete components and distributed transmission line elements was used as shown in Fig. 9 since it allows for easy tuning of the matching network based on the RF-dc's response to varying input power levels and output loads. The matching network was optimized for the power levels measured at "E" 6.3 km away from the TV broadcast source. The extra phase introduced by the SMA

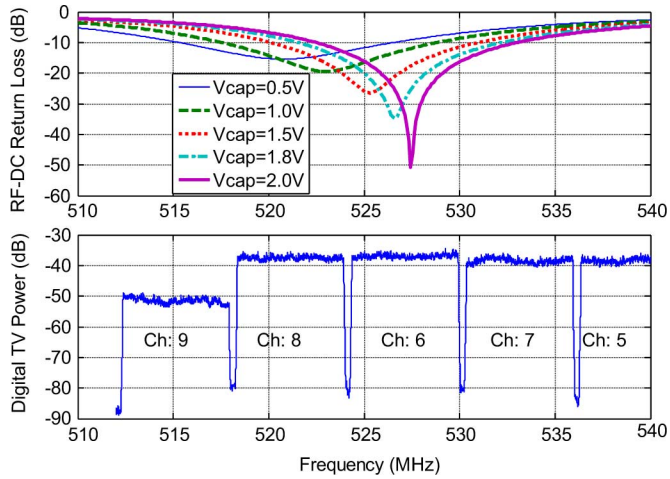

Fig. 12. Measured E-WEHP RF to dc charge-pump input return loss $[S_{11}(f, V_{\text{CAp}})]$ for charge-tank capacitor voltage (V_{CAp}) between 0.5–2.0 V with respect to the wireless digital TV channels measured in the field.

connectors are included as part of the distributed transmission-line network. Capacitors of 1 and 6.6 pF for CS1 and CS2 along with the added phase of microstrip to SMA input transition to give a return-loss bandwidth of 12 MHz over the TV frequency bands. However, by using a multi-section matching and a shorter transmission-line network, the overall return-loss bandwidth can be increased up to a maximum of 71 MHz, which is the theoretical Bode-Fano limit for the RF-dc's reactive loads at the TV bands [28].

As the RF-dc charge-tank voltage increases, the matching circuit ensures that the charge-pump's varying impedance is conjugately matched to the 50-Ω log-periodic antenna over digital-TV frequency channels, as shown in Fig. 12. The matching network design of the E-WEHP is optimized such that during the initial charge up of the charge-tank capacitor at 0.5 V, its return loss (S_{11}) in (2) is greater than 10 dB at frequencies between 515–527 MHz, at which point the E-WEHP harvests power from digital TV channels #9 (JOMX) and #8 (JOCX), as shown in Fig. 12. Ensuring over 90% power transfer from one or more ambient wireless TV channels at initial turn-on is critical to ensure further charge build up across the charge-tank capacitor. As charge-tank voltage varies between 1.8–2.0 V, the matching network is designed to have a return loss (S_{11}) greater than 10 dB between wireless TV channels 8, 6, and 7, where peak ambient wireless power is transduced by the log periodic antenna, as shown in Fig. 12. This ensures maximum power harvesting from the ambient signals and charge flow into the charge-tank capacitor to replenish it when the E-WEHP's PIC24F enters the charge/sleep mode covered in a subsequent section.

C. RF-DC Charge-Pump Turn-on Power and Efficiency

In order to characterize the E-WEHP RF-dc charge-pump's response to multi-carrier and multi-channel signals present in the air, a Rohde and Schwarz SMJ100A RF vector signal generator (SigGen) and a Tektronics RSA 30408A real time spectrum analyzer (RTSA) are used to emulate the Digital TV signals in the laboratory. The RF-dc charge-tank's output voltage is

measured with a Tektronics DPO7354 oscilloscope with a high-impedance probe. Peak envelope power limits of the SigGen do not allow generating 5567 subcarriers across each of the nine TV channels that are present under ISDB-T digital TV standards measured in the field in Fig. 7. However, using 1860 carriers, each 29 kHz apart for a baseband signal around a carrier frequency of 539 MHz with a chirp-type power distribution scheme, a nine TV-channel-wide signal with roughly the same channel power as in the field is emulated in the laboratory without exceeding the peak envelope power limit of the Rohde SigGen, albeit with lower subcarrier amplitude, as shown in Fig. 7.

The E-WEHP is tested in the laboratory with the emulated multi-carrier RF signal for different channel power levels with a 1- and 18-MΩ load across the E-WEHP's output charge-tank. The loads emulate a PIC24F 16-bit embedded microcontroller operating in deep-sleep mode on 32-kHz clock speed, which is when the E-WEHP would be transferring incoming wireless power from the air into the charge-tank capacitor for limited duty cycle operations. Since the wireless power harvested from the air is not continuously powering the load, but by using a collect first (charge/sleep) and use later (discharge/active) mechanism, we use the relationship in (5) to gauge the energy efficiency of the E-WEHP's RF-dc charge-pump circuit.

In (5), the energy collected by the E-WEHP RF-dc charge-pump is dependent on the charge-tank capacitance (C_L) and voltage $(V_{\rm cap})$. The energy supplied by the ambient wireless TV signals through the log periodic antenna is the total input channel power (PCHANNEL) across all nine TV channels during the time taken by the charge-pump to charge to 1.8 V $(T_{\rm VCAP})$. Calculating efficiency in terms of energy, which is a function of power and time, is a better gauge of the energy-harvesting efficiency of the E-WEHP given the multi-channel make up of digital TV signals and E-WEHP's time-varying response to it based on the charge-tank's voltage, as shown in Fig. 12.

However, the charge build-up at the charge-tank is only due to the input power contained in two TV channels due to the 12-MHz return-loss bandwidth of the RF-dc charge-pump circuit. The efficiency of the E-WEHP's RF-dc charge-pump only with respect to the input power within two TV channels causing the charge up is determined using (6), where the term "$P\neg 2$ CHANNELS" is the channel power contained within two TV channels. The efficiency of the E-WEHP for an output charge-tank voltage ($V_{\rm CAP}$) of 1.8 V for output loads of 1 and 18 MΩ using (6) are shown in Fig. 13 with respect to the total input channel power across all nine digital-TV channels.

Energy efficiency of the E-WEHP RF-dc charge-pump circuit fed with digital TV signals emulated in the laboratory show maximum efficiencies of 19.50% and 21% for 1- and 18-MΩ loads across the charge-tank capacitor, respectively. Around total channel power levels of −8.99 dBm (126 mW) that is present at 6.3 km from the TV source, laboratory tests on the E-WEHP yield efficiencies of between 55%–15% for 1- and 18-MΩ output loads across the charge-tank capacitor, respectively. Output voltage measurements on the E-WEHP under laboratory conditions with a Tektronics oscilloscope

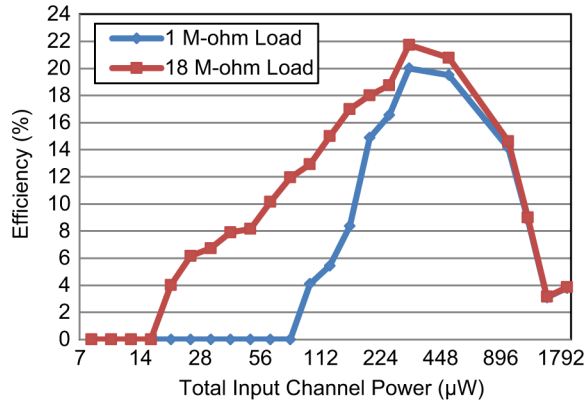

Fig. 13. E-WEHP RF-dc energy conversion efficiency versus input channel power.

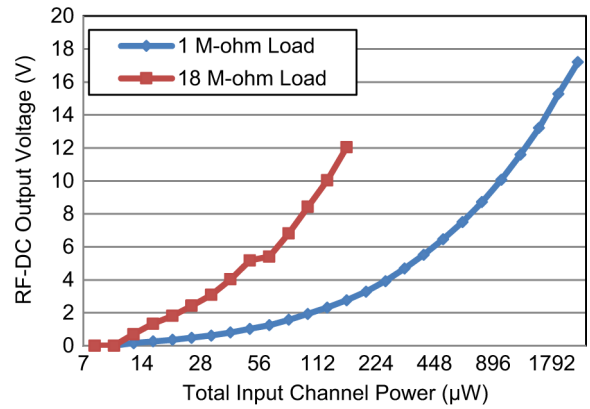

Fig. 14. E-WEHP RF-dc output charge-tank voltage versus input channel power.

(Scope) show the E-WEHP's 100 μF charge-tank voltage rise to 2.32 V in 406 s for a 1-MΩ load with an input channel power level of around −8.99 dBm (126 mW), as shown in Fig. 14. The E-WEHP gives out a higher voltage in excess of 10.32 V for the same input channel power with an 18-MΩ load across the charge-tank

$$\eta_{\rm ALL-CHANNELS} = \frac{\text{Energy output}}{\text{Energy in all channels}} = \frac{\frac{1}{2}\cdot C\cdot V_{\rm CAP^2}}{P_{\rm All-channels}\cdot T_{VCAP}}\cdot 100 \quad (5)$$

$$\eta_2 = \frac{\text{Energy out}}{\text{Energy in two channels}} = \frac{\frac{1}{2}\cdot C_L\cdot V_{\rm CAP^2}}{P_2-\text{CHANNELS}\cdot T_{VCAP}}\cdot 100. \quad (6)$$

VII. Field Performance

The E-WEHP prototype is tested in the field by orienting its log-periodic antenna toward the digital-TV broadcast sources atop the Tokyo TV 6.3 km away, as shown in Figs. 3 and 15. The E-WEHP's 100-μF charge-tank output charges up to 4.18 V in

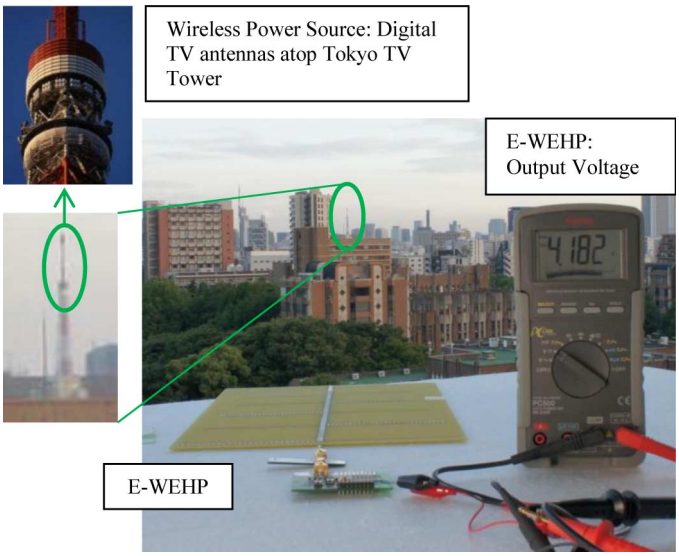

Fig. 15. Field measurement in downtown Tokyo, Japan, with E-WEHP prototype harvesting wireless energy from multi-carrier wireless digital TV signals broadcasted from atop the Tokyo TV tower 6.3 km away.

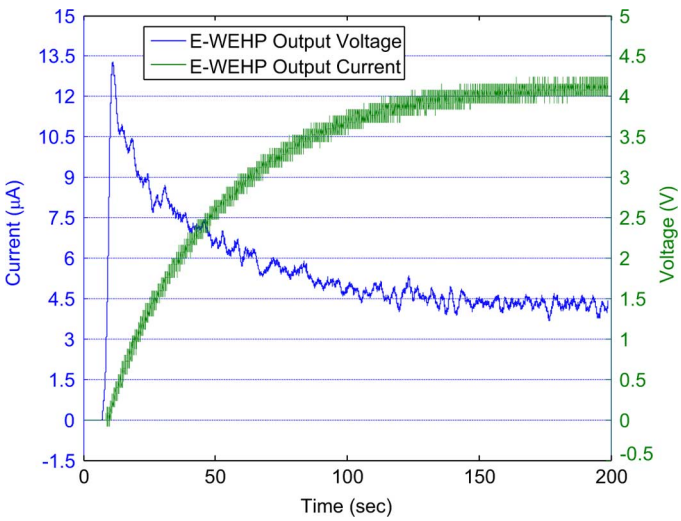

Fig. 16. E-WEHP output voltage and current measured at the POI after filtering out higher frequency noise ripples introduced by the environment and the E-WEHP RF-dc charge-pump circuit.

120 s from the ambient wireless TV signals, as shown by oscilloscope measurement in Fig. 16. Higher output voltage in the field in a shorter period of time compared to laboratory measurement is primarily due to the ambient TV signals having a higher crest factor (peak-to-average power ratio) while still having the same channel power compared to the RF test signal emulated in the laboratory, as seen in Fig. 7.

In the field, wireless TV signals received by the E-WEHP antenna have maximum carrier levels of −37 dBm (158.5 nW) (TV channel numbers: 8, 6, 7, 5, 2, and 1) and minimum carrier levels of −50 dBm (TV channel #9) to yield a total channel power level across all nine TV channels of −8.99 dBm including the nulls in between each of the TV channels, as shown in Fig. 7. By comparison, the TV signals emulated in the laboratory using the SigGen has peak carrier levels limited to −41.42 dBm (72.1 nW) across all nine channels to yield roughly the same channel power level of −8.95 dBm in order not to exceed the SigGen's peak envelope power limit, as shown in Fig. 7. Higher amplitude tones at the input of the RF-dc charge-pump have the effect of lowering the loss across each of its Schottky diodes resulting in higher amounts of wireless trickle charge flowing into the charge-tank, thereby resulting in higher output voltage and conversion efficiency in the field.

The E-WEHP's output current sourced from the ambient wireless TV signals is the sum of the current charging up the E-WEHP's charge-tank capacitor $(C_L \cdot dV_{\rm CAP}/dt)$, the current consumed by any load across the charge-tank and current leakages through the load and charge-tank $(I_{\rm c-LEAK})$, as in (7). In (7), $I_{\rm MCU}$ is the current consumed by the end load comprised of an embedded microcontroller and $\rm V_{CAP}/R_{PROBE}$ is the current consumed by the high-impedance scope probe used to measure the E-WEHP's output charge profile. The Tektronics high-impedance probe used to measure E-WEHP performance at long distances from the source has an impedance of 1 MΩ $(R_{\rm PROBE})$, and introduces leakage of the order of microamperes at the E-WEHP output, which has to be accounted for such LP measurements

$$I_{\text{E-WEHP}} = C_L \cdot \frac{dV_{\rm CAP}}{dt} + I_{C-\rm LEAK} + \frac{V_{\rm CAP}}{R_{\rm PROBE}} + I_{\rm MCU}. \quad (7)$$

The E-WEHP output voltage typically saturates to a maximum, when its harvested wireless trickle charge current equals the current consumed in the load across the charge-tank plus current leakages in the charge-tank, load, and measurement probes at the RF-dc output. The E-WEHP's output voltage and charge profile current measured in the field is shown in Fig. 16. The E-WEHP's dc output current was filtered using a low-pass moving average filter with a time span of 1.6 s to filter out noise ripples, which is necessary to enable current measurements in the range of microamperes, as shown in the current plot in Fig. 16. In the field, 6.3 km from the wireless TV broadcast source, the E-WEHP is capable of continuously sourcing between 4.1–8.25 mA at output voltages of between 4.1–1.8 V, respectively, as seen in Fig. 16. At these output voltages, total output power given by the E-WEHP is between 15–17 mW, which translates to an RF-dc efficiency between 26.2%–29.7% in the field. The E-WEHP output saturates to 4.1 V when its output current draw is equal to the 4.1 mA, which is the current consumed through the 1-MΩ oscilloscope probe.

VIII. Wireless TV-Signal-Powered Embedded Device

In almost every sensing application, embedded microcontrollers play a vital role in sampling, processing, recording, and relaying sensed information to the outside world through M2M networks. At the time of this research, a comparison of voltage and current ratings of lowest power microcontrollers was done, which are shown in Table IV. Most embedded microcontrollers require between 1.8–3.6 V [36]–[38] to operate where most CMOS processes offer the optimum combination of low-voltage and low-current leakage. Newer microcontrollers typically consume in the order of milliamperes at megahertz or higher clock speeds and tens of microamperes at lower kilohertz clock speeds. The latest microcontrollers also offer extreme LP sleep modes that consume currents in the order of

TABLE IV
MICROCONTROLLER ELECTRICAL SPECIFICATIONS

Microcontroller	Clock Speed	Operating Voltage Range	Current
Microchip PIC24F	32 MHz	1.8 - 3.6 V	11 mA
	32 kHz	1.8 - 3.6 V	8-15 uA
	LP Deep Sleep	1.8 - 3.6 V	20-800 nA
TI MSP430	16 MHz	1.8 - 3.6 V	7 mA
	4 kHz	1.8 - 3.6 V	5-6 uA
	LP LPM4	1.8 - 3.6 V	100-150 nA
Silicon Labs SiM3C1XX	80 MHz	1.8 - 3.6 V	33 mA
	16.4 kHz	1.8 - 3.6 V	175-250 uA
	LP P.Mode9	1.8 - 3.6 V	85-650 nA

tens to hundreds of nanoamperes with use of limited memory and peripherals [36]–[38].

A comparison of the E-WEHP's wireless power sourcing capabilities and the microcontroller electrical specifications, in Fig. 16 and Table IV, respectively, show that at lower clock speeds in the kilohertz range or in the LP sleep modes, the E-WEHP can power up limited embedded applications consuming between 20 nA-8 μA, while still allowing output voltages of between 1.8–4 V, respectively. At long ranges, the E-WEHP cannot supply milliamperes of current for high-speed embedded operations in the megahertz range. However, reserve energy stored in the E-WEHP's charge-tank capacitor is successfully used to power high-speed operations for limited duty cycles by using a collect first (sleep/charge mode), and use later (active/discharge mode) embedded scheme.

A microchip 16-bit PIC24F16KA101 microcontroller unit (MCU) is programmed with an energy-aware software design to sustain itself using just the ambient wireless power present in digital TV signals without the aid of any batteries or significant power-management electronics. The PIC24F microcontroller includes nine 10-bit analog-to-digital converter (ADC) modules; a real time clock and calendar (RTCC) module; two watch dog timers (WDTs); a high–low-voltage detect (HLVD) module; limited sleep memory retention; and several CPU interrupting schemes. The MCU peripherals are successfully used for a software-based power-regulation and management scheme to sustain ADC sampling, time stamping, and serial UART communication functions using just microwatts of harvested wireless TV-signal power flowing into the 100-μF charge-tank capacitor. The hardware configuration of the microcontroller in the E-WEHP system can be seen in Figs. 8 and 9. The software algorithm successfully used to run of the ambient wireless power is carried out in three different MCU operating modes outlined in subsequent sections.

A. Power-Up Mode

At initial power up, the digital field-effect transistor (FET)-based switches in most processors are neither in an ON, nor OFF state, which results in the processor inputs/outputs (I/Os) leaking substantial amounts of current. Several options propose the use of a battery to bootstrap the power-up operation or operate the energy harvesters at close range from the wireless source [21], [39]. The E-WEHP does not use a battery or extensive power-management hardware, but instead relies on a

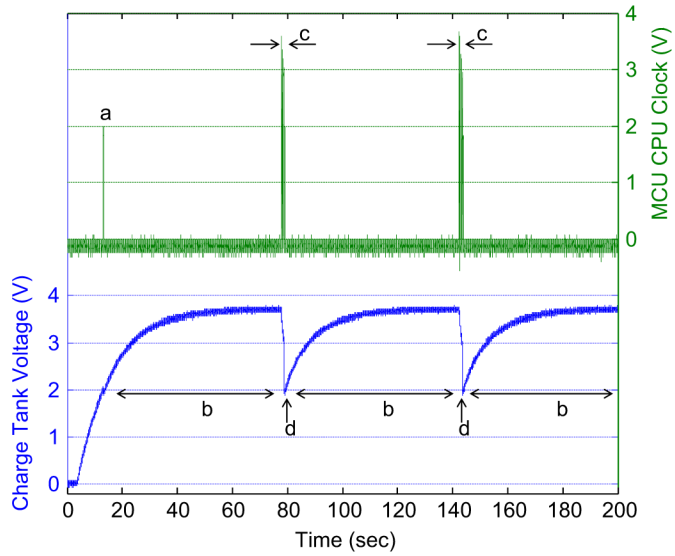

Fig. 17. Self-sustaining E-WEHP's embedded MCU operation powered with ambient wireless digital TV signals with channel power of −8.99 dBm present 6.3 km from broadcast source in Tokyo, Japan. (a) Power up mode. CPU Clock = 8 MHz. (b) Charge/sleep mode. RTCC on, CLK = 32 kHz, 60-s wake-up interval. (c) Active/discharge mode: 2-s duty cycle, RTCC, ADC, UART, LED, Ext INT on, CLK = 32 kHz − 8 MHz. (d) Transition from active to charge mode triggered by external interrupt at charge-tank voltage of 1.9 V.

software-based approach to power up from the energy stored in the 100-μF charge-tank capacitor. While some of the leakages during power-up may be unavoidable, using a faster clock can cut down this leakage time substantially. On the PIC24F MCU, an 8-MHz start-up clock was used to wake up the CPU in 1–10 ms. By comparison, a 32-kHz clock wakes up the CPU in 300 ms [37]. A faster startup avoids deep discharge of the 100-μF charge-tank by the MCU during initial boot-up. Once the MCU CPU is up and running at an 8-MHz clock, its I/O pins were programmed as outputs and latched to a high or "1" state to prevent them from siphoning off any charge from the 100-μF charge-tank. The I/O pins that could be configured as analog I/Os were programmed as inputs since they offered the highest input impedance helping arrest the charge-tank leakage further. Once I/O leakages were plugged, the MCU was programmed to slow down its CPU clock speed from 8 MHz to a lower 32 kHz using software to minimize current consumption from 2.25 mA to 8 μA; hence, slowing down current discharge during the power-up sequence [37]. Next, the external interrupt and RTCC module in the MCU were configured for voltage supervision of the charge-tank and time stamping of any sensed data. All of the remaining modules of the MCU were turned off in software, and the MCU was then programmed to put itself into an ultra-LP sleep/charge state, which allows the charge-tank to replenish itself for the losses during initial boot-up from the ambient wireless power, as shown by stage a in Fig. 17.

B. Sleep/Charge Mode

Most sensing applications require the sensor to be sampled only at intervals of seconds to hours or longer. In between the sensor readings, the interrogating microcontroller can be turned off or put in a hibernating state to conserve power. The MCU

was programmed to go into a deep sleep mode after power-up and in between sensor interrogations with its real time clock calendar (RTCC) module enabled. This allows the capability to time stamp any sensor reading while still consuming currents of between 490–800 nA, which along with the leakage through the oscilloscope probe of around 4.5 μA still allows the E-WEHP's charge-tank capacitor to charge up to around 3.75 V from the ambient wireless power present in the field as per the E-WEHP's charge profile shown in Fig. 16. The charge-tank's charge profile during sleep/charge mode is shown by stage b in Fig. 17. In the field, 6.3 km from the TV broadcast source, the E-WEHP required close to 66 s to refill its charge-tank from 1.9 to 3.75 V using the wireless power in the air. The MCU was therefore programmed to wake itself up from deep-sleep mode at chimed intervals of every 60 s after entering deep-sleep mode using the RTCC clock at which point the MCU firmware was programmed to activate itself or any attached sensor to get into the active mode. An embedded algorithm to detect the optimum wake-up time based on the E-WEHP's distance from the TV broadcast source has also been implemented, but will be covered in a subsequent publication due to page limits.

C. Active/Discharge Mode

In active mode, the MCU is programmed to turn on the CPU in order to activate its peripherals, namely, the ADC and universal asynchronous (UART) modules, to carry out most kinds of analog sensor sampling and M2M communication with an LP radio transceiver or a host PC for wireless telemetry of sensed data. ADCs and UART modules in the PIC24F consume roughly between 200 μA–1 mA each, respectively, which is larger than the current flow generated from the ambience by the E-WEHP in the field 6.3 km from the broadcast source, as shown in Fig. 16. This causes its charge-tank capacitor to supply the excess current from its charge stored in the previous sleep/charge mode cycle, and in the process discharging itself. Using just firmware with very minimal empirically designed hardware, the MCU is programmed to prevent deep discharge of the charge-tank capacitor down to below 1.8 V where MCU gets latched onto a never-ending reset state.

Deep discharge of the charge-tank is arrested through the use of resistors R1 and R2, diode D12, and the MCU's external interrupt module programmed at its INT0/RB7 input pin, as shown in the schematic in Fig. 8. 40-MΩ resistors were used for R1 and R2, respectively, which in parallel with the input impedance of the MCU's external-interrupt input pin, produces a voltage of 1.8 V at the input when the charge-tank capacitor discharges to 1.9 V. A high to low transition at the INT0/RB7 input is programmed to interrupt the MCU's CPU from any ongoing ADC or UART operation, power down the peripherals and I/Os, and put the MCU back into sleep/charge mode with only the RTCC module on as shown by stage d in Fig. 17. A Diode "12" with a high forward voltage is used to delay leakage of charge-tank current through the resistors during its initial charge up. The current consumed by the external interrupting embedded scheme is 82.5 nA, which is much lower than 10 s of μAs consumed by power management integrated circuits (ICs) during initial charge up. Embedded operations, including any

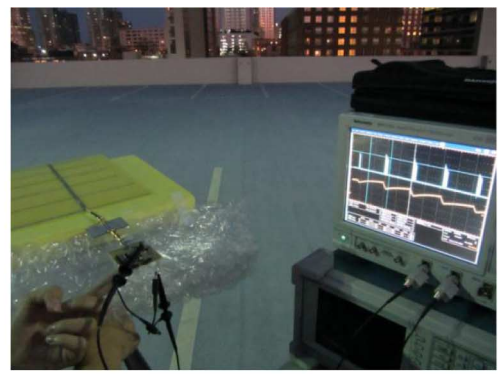

(a)

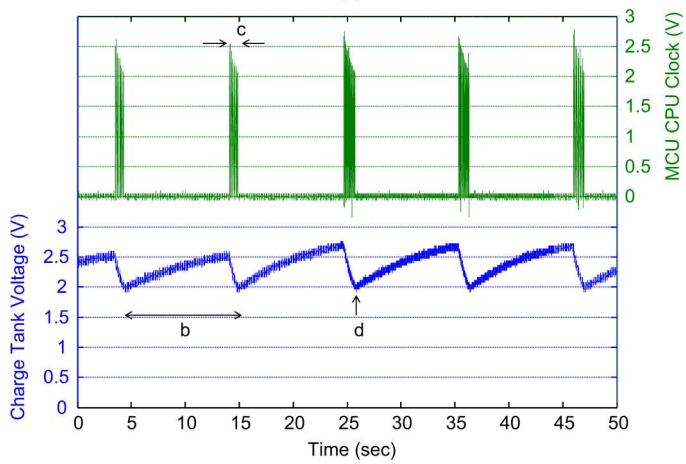

(b)

Fig. 18. (a) and (b) Self-sustaining E-WEHP embedded operation powered with input wireless channel power of -13.92 dBm present in wireless TV signals in Atlanta, GA, USA. b: Charge/sleep mode. RTCC on, CLK $= 32$ kHz, 10-s wakeup interval. c: Active/discharge mode: 2-s duty cycle, RTCC, ADC, UART, LED, Ext INT on, CLK $= 32$ kHz $-$ 8 MHz. d: Transition from active to charge mode triggered by external interrupt at charge-tank voltage of 1.9 V.

sensing function, is carried out in the amount of time taken by E-WEHP's 100-μF charge-tank to discharge from its maximum output voltage to 1.9 V at which point the external interrupt is triggered putting MCU in the sleep/charge mode, as shown by stage c in Fig. 17.

The time interval over which the MCU is operational in the active/discharge mode (T_{ON}) is a function of the charge-tank capacitance (C_L); the maximum voltage generated by the E-WEHP's RF-dc charge-pump $(v_{\mathrm{CAP\text{-}MAX}})$ from the ambient wireless power, which is a function of the E-WEHP's range from the TV broadcast source; the MCU's turn off voltage $(V_{\mathrm{MCU\text{-}OFF}})$; and the current consumed by the MCU's peripherals that are turned on (I_{MCU}), which can be estimated using (8) [40]. Depending on the CPU clock and the peripherals turned on in the active mode, the operating duty cycle of the E-WEHP is expected to be between 6.1 ms–12.2 s, during which the MCU executes between 48 800–390 400 instructions at clock speeds of 8 MHz and 32 kHz, respectively, with the ADC, RTCC, UART, and external interrupt peripherals running under software control. For the operation in Fig. 17, 51 bytes of UART, a 10-bit ADC module, and an LED consuming 2.5 mA were powered on for a 2-s window using the wireless power

harvested from the air without batteries at 6.3 km from the digital TV broadcast source

$$T_{\mathrm{ON}} = -\ln\left(\frac{V_{\mathrm{MCU\text{-}OFF}}}{V_{\mathrm{CAP\text{-}MAX}}}\right) \cdot \frac{V_{\mathrm{MCU\text{-}OFF}} + V_{\mathrm{CAP\text{-}MAX}}}{2 \cdot I_{\mathrm{MCU}}} \cdot C_L. \tag{8}$$

In addition to harvesting power from ISDB-T digital TV signals in Japan, an optimized version of the E-WEHP was also designed for harvesting power from wireless TV signals in the U.S. that use the ATSC standard for terrestrial wireless TV broadcasts. The optimized E-WEHP prototype has an RF-dc single carrier sensitivity of -18.86 dBm (13 μW), and generates 3.26-V output from multi-carrier ATSC TV signals with channel power of 40.55 mW (-13.92 dBm) and carrier levels of 0.063 μW (-42 dBm) across two 6-MHz-wide TV channels (CBS and IND) broadcasted out from a source 5.6 km away. The energy-efficient E-WEHP algorithm was also tested in the field in Atlanta, GA, USA, and showed the PIC24F MCU being able to sustain itself perpetually from even lower levels of ambient wireless power at long distance from the CSB and IND TV broadcast sources with wake-up time intervals of 10 s in the sleep/charge mode, as shown in Fig. 18.

IX. Conclusion

A novel wireless energy-harvesting mechanism to power-on and sustain embedded microcontroller-based sensing operations using ambient wireless digital-TV signals has been presented. By carefully characterizing and targeting the multi-carrier make up of modern digital TV signals present in most urban areas, an optimized log-periodic antenna, an RF-dc charge-pump circuit, and an energy-aware embedded firmware have been developed to sustain embedded microcontrollers at long range from the wireless broadcast source. By using an optimized log-periodic antenna with peak gain of 7.3 dBi, and an RF-dc charge-pump circuit with carrier RF-dc sensitivity of -14.6 dBm (4.67 μW), sensing peripherals on a 16-bit PIC24F microcontroller are successfully powered from TV signals with peak carrier levels of -7 dBm (0 W) and channel power levels of -8.99 dBm (126.2 μW) at 6.3 km from the source in downtown Tokyo, Japan. Using an improved RF-dc charge-pump with single-carrier RF-dc sensitivities of -18.86 dBm (13 μW), a 16-bit PIC24F microcontroller is successfully powered from even lower levels of ATSC standard-based wireless TV signals with channel power levels of 40.55 mW (-13.92 dBm) and carrier levels of 0.063 μW (-42 dBm) that are prevalent in the U.S. Such a self-powering platform to power on embedded sensors make it highly suitable for a number of applications such as smart metering, structural health monitoring, and environmental sensing where the logistics of battery replacement prove to be expensive or inaccessible.

References

[1] R. Vyas *et al.*, "A battery-less, energy harvesting device for long range scavenging of wireless power from terrestrial TV broadcasts," in *IEEE MTT-S Int. Microw. Symp. Dig.*, Montreal, QC, Canada, Jun. 2012, pp. 1–3.

[2] K. Finkenzeller, *RFID Handbook*, 2nd ed. New York, NY, USA: Wiley, 2003, ch. 9, pp. 271–271.

[3] D. Schneider, "A critical look at wireless power," *IEEE Spectr.* May 2010.

[4] G. A. Covic and Y. X. J. T. Boys, "DC analysis technique for inductive power transfer pick-ups," *IEEE Power Electron. Lett.*, vol. 1, no. 2, pp. 51–53, Jun. 2003.

[5] J. T. Boys, M. L. G. Kissin, and H. G. L. G. A. Covic, "A three-phase inductive power transfer system for roadway-powered vehicles," *IEEE Trans. Ind. Electron.*, vol. 54, no. 6, pp. 3370–3378, Dec. 2007.

[6] W. Lee, G. Cho, B. Lee, and C. R. J. Huh, "Characterization of novel inductive power transfer systems for on-line electric vehicles," in *IEEE Appl. Power Electron. Conf. and Expo.*, 2011, pp. 1975–1979.

[7] S. Ahn *et al.*, "Low frequency electromagnetic field reduction techniques for the on-line electric vehicle (OLEV)," in *IEEE Int. Electromagn. Compat. Symp.*, 2010, pp. 625–630.

[8] J. D. Joannopoulos, M. Soljacic, and A. Karalis, "Efficient wireless non-radiative midrange energy transfer," *Ann. Phys.*, vol. 323, pp. 34–48, 2008.

[9] D. T. Emerson, "The work of Jagadish Chandra Bose: 100 years of mm wave research," *IEEE Trans. Microw. Theory Techn.*, vol. 45, no. 12, pp. 2267–2273, Dec. 1997.

[10] J. A. Hagerty, F. B. Helmbrecht, W. H. McCalpin, R. Zane, and Z. B. Popovic, "Recycling ambient microwave energy with broadband rectenna arrays," *IEEE Trans. Microw. Theory Techn.*, vol. 52, no. 3, pp. 1014–1024, Mar. 2004.

[11] K. Tashiro, H. Wakiwaka, S. Inoue, and Y. Uchiyama, "Energy harvesting of magnetic power-line noise," *IEEE Trans. Magn.*, vol. 47, no. 10, pp. 4441–4444, Oct. 2011.

[12] Y. Zhang *et al.*, "A batteryless 19 μW MICS/ISM-band energy harvesting body sensor node soc for EXG applications," *IEEE J. Solid-State Circuits*, vol. 48, no. 1, pp. 199–213, Jan. 2013.

[13] C. Sauer *et al.*, "Power harvesting and telemetry in CMOS for implanted devices," *IEEE Trans. Circuits Syst.*, vol. 52, no. 12, pp. 2605–2613, Dec. 2005.

[14] J. Pandey *et al.*, "A fully integrated RF-powered contact LENS with a single element display," *IEEE Trans. Biomed. Circuits Syst.*, vol. 4, no. 6, pp. 454–461, Dec. 2010.

[15] H. Reinisch *et al.*, "An electro-magnetic energy harvesting system with 190 nW idle mode power consumption for a baw based wireless sensor node," *IEEE J. Solid-State Circuits*, vol. 46, no. 7, pp. 1728–1741, Jul. 2011.

[16] J. Yin *et al.*, "A system-on-Chip EPC gen-2 passive UHF RFID tag with embedded temperature sensor," *IEEE J. Solid-State Circuits*, vol. 45, no. 11, pp. 2404–2420, Nov. 2010.

[17] D. Yeager *et al.*, "A 9 uA, addressable Gen2 sensor tag for biosignal acquisition," *IEEE J. Solid-State Circuits*, vol. 45, no. 10, pp. 2198–2209, Oct. 2010.

[18] U. Karthaus and M. Fischer, "Fully integrated passive UHF RFID transponder IC with 16.7-μW minimum RF input power," *IEEE J. Solid-State Circuits*, vol. 32, no. 10, pp. 1602–1608, Oct. 2003.

[19] "RF energy harvesting and wireless power," Powercast Corporation, Pittsburgh, PA, USA, Apr. 2012. [Online]. Available: http://www.powercastco.com/PDF/powercast-overview.pdf

[20] "EPC Global, EPC Radio-Frequency Identification Protocols Class-1 Generation-2 UHF RFID EPC Protocol for Communications at 860–960 MHz," EPC Global Inc., Lawrenceville, NJ, USA, 2008, vers. 1.2.0, 23.

[21] A. Dolgov, R. Zane, and Z. Popovic, "Power management system for online low power RF energy harvesting optimization," *IEEE Trans. Circuits Syst. I, Reg. Papers*, vol. 57, no. 7, pp. 1802–1811, Jul. 2010.

[22] J. S. A. Sample, "Experimental results with two wireless power transfer systems," in *Radio Wireless Symp.*, Jan. 2009, pp. 16–18.

[23] "SRM 3000 selective radiation meter datasheet," NARDA, Chicago, IL, USA, 2012.

[24] D. Sparano, "What exactly is 8-VSB anyway?," ARRL, Newington, CT, USA, 1997. [Online]. Available: http://www.arrl.org/files/file/Technology/TV_Channels/8_Bit_VSB.pdf

[25] "DTV ISDB OFDM project example," Agilent Technol., Santa Clara, CA, USA, 2005. [Online]. Available: http://cp.literature.agilent.com/litweb/pdf/ads2005a/dtv/dtv124.html

[26] "Outline of the specification for ISDB-T" NHK Japan Broadcast. Corporation, Tokyo, Japan, 1999. [Online]. Available: http://www.nhk.or.jp/strl/open99/de-2/shosai-e.html

[27] J. S. Seybold, *Introduction to RF Propagation*. New York, NY, USA: Wiley, 2005, ch. 7, pp. 134–162.

[28] D. Pozar, *Microwave Engineering*. New York, NY, USA: Wiley, 2005.
[29] "Spectral measurements—Part 1. White paper," Nat. Instrum., Austin, TX, USA, Jan., 2012. [Online]. Available: http://www.ni.com/white-paper/4146/en
[30] D. Isbell and R. Duhamel, "Broadband logarithmically periodic antenna structures," in *IRE Int. Conv. Rec.*, 1957, pp. 119–128.
[31] R. Carrel, "Analysis and design of the log-periodic dipole antenna," Elect. Eng. Res. Lab., Univ. Illinois at Urbana–Champaign, Urbana, IL, USA, Tech. Rep., 1961.
[32] C. Balanis, *Antenna Theory*. New York, NY, USA: Wiley, 1997, ch. 11, pp. 569–588.
[33] G. D. Vita and G. Iannaccone, "Design criteria for the RF section of UHF and microwave passive RFID transponders," *IEEE Trans. Microw. Theory Techn.*, vol. 53, no. 9, pp. 2978–2990, Sep. 2005.
[34] P. Pannier, J. Gaubert, and E. Bergeret, "Optimization of UHF voltage multiplier circuit for RFID application," *IEEE Trans. Circuits Syst. II, Exp. Briefs*, vol. 8, no. 12, pp. 13–15, Dec. 2005.
[35] P. Pannier, J. Gaubert, J. Gaultier, and E. Bergeret, "Modeling and design of CMOS UHF voltage multiplier for RFID in an EEPROM compatible process," *IEEE Trans. Circuits Syst. II, Exp. Briefs*, vol. 10, pp. 833–837, Oct. 2007.
[36] "TI MSP430F2274 mixed signal microcontroller datasheet," Texas Instrum. Incorporated, Dallas, TX, USA, Data Sheet, Jul. 2011. [Online]. Available: www.ti.com
[37] "PIC24F16KA102 family datasheet," Microchip Technol. Inc., Chandler, AZ, USA, 2009. [Online]. Available: http://ww1.microchip.com/downloads/en/DeviceDoc/PIC24F16KA102_Family_datasheet_39927b.pdf,
[38] "SiM3C1xx high-performance, low-power, 32-bit precision32 MCU family with up to 256 kB of flash datasheet," Silicon Labs., Austin, TX, USA, 2012. [Online]. Available: http://www.silabs.com/Support%20Documents/TechnicalDocs/SiM3C1xx.pdf
[39] A. P. Sample, D. J. Yeager, P. S. Powledge, A. V. Mamishev, and J. R. Smith, "Design of an RFID-based battery-free programmable sensing platform," *IEEE Trans. Instrum. Meas.*, vol. 57, no. 11, pp. 2608–2615, Nov. 2008.
[40] R. Vyas, V. Lakafosis, Z. Konstas, and M. M. Tentzeris, "Design and characterization of a novel battery-less, solar powered wireless tag for enhanced-range remote tracking applications," in *Eur. Microw. Conf.*, 2009, pp. 169–172.
[41] N. Tran, B. Lee, and J.-W. Lee, "Development of long-range UHF-band RFID tag chip using Schottky diodes in standard CMOS technology," in *IEEE RF Integr. Circuits Symp.*, Honolulu, HI, USA, 2007, pp. 281–284.
[42] P. Nintanavongsa, U. Muncuk, D. R. Lewis, and K. R. Chowdhury, "Design optimization and implementation for RF energy harvesting circuits," *IEEE J. Emerg. Select. Topics Circuits Syst.*, vol. 2, no. 1, pp. 24–33, Mar. 2012.
[43] G. Hugo, "Nikola Tesla and his achievements," *Elect. Experimenter*, pp. 615–615, Jan. 1919.
[44] P. V. Nikitin, K. V. S. Rao, R. Martinez, and S. F. Lam, "Sensitivity and impedance measurements of UHF RFID chips," *IEEE Trans. Microw. Theory Techn.*, vol. 57, no. 5, pp. 1297–1302, May 2009.

Rushi J. Vyas (M'06) received the B.S. and M.S. degrees in electrical engineering from the Georgia Institute of Technology, Atlanta, GA, USA, in 2005 and 2010, respectively, and is currently working toward the Ph.D. degree at the Georgia Institute of Technology.

He is currently a Researcher with the ATHENA Research Group, Georgia Institute of Technology. He has authored or coauthored over 27 research publications in peer-reviewed journals and conference proceedings and two book chapters covering topics such as RF energy-harvesting, inkjet-printed electronics, wireless sensors and RTLS systems. His research on RF-energy harvesting and batteryless sensors have also been covered in media forums such as MSN news, *Engadget*, *IEEE Institute*, *Energy Harvesting Journal*, and *New Energy and Fuel*.

Dr. Vyas was a finalist and honorable mention awards of the IEEE Microwave Theory and Techniques Society (IEEE MTT-S) International Microwave Symposium (IMS) 2008 and 2012 and the IEEE Antennas and Propagation Society (AP-S) 2008 and 2009 conferences. He was the recipient of the 2012 ICMG Architecture IT Excellence Award for his doctoral work.

Benjamin B. Cook received the Bachelor's degree in electrical engineering from the Rose-Hulman Institute of Technology, Terre Haute, IN, USA, in 2010, the Masters degree in electrical engineering from King Abdullah University of Science and Technology, Thuwal, Saudi Arabia, in 2011, and is currently working toward the Ph.D. degree in electrical engineering at the Georgia Institute of Technology, Atlanta, GA, USA.

He has authored or coauthored over 20 publications in peer-reviewed journals and conferences. His research focuses are in multilayer millimeter-wave frequency device fabrication using inkjet printing on polymer and organic substrates, system-on-paper applications, green electronics, and microelectromechanical systems (MEMS) device fabrication.

Mr. Cook was the recipient of the Outstanding Senior Engineer of the Year Award in 2010, the KAUST Fellowship Award in 2010, the KAUST Provost Award in 2011, and the IEEE Antennas and Propagation Society (AP-S) Doctoral Research Award for his work in inkjet-printed flexible and conformal antennas and passive components.

Yoshihiro Kawahara (S'01–M'05) received the B.E. degree, M.E. degree, and Ph.D. degree in information communication engineering from the University of Tokyo, Toyko, Japan, in 2000, 2002, and 2005, respectively.

He is currently a Lecturer with the Department of Information and Communication Engineering, University of Tokyo, Tokyo, Japan. His research interests are in the areas of computer networks and ubiquitous and mobile computing. In 2005, he joined the faculty of the University of Tokyo. He is a Visiting Scholar with the Georgia Institute of Technology, Atlanta, GA, USA.

Dr. Kawahara is a member of the Institute of Electronics, Information and Communication Engineers (IEICE), Japan and the Information Processing Society of Japan (IPSJ). He's a committee member of IEEE MTT TC-24 (RFID Technologies.)

Manos M. Tentzeris (S'89–M'92–SM'03–F'10) received the Diploma degree in electrical and computer engineering (*magna cum laude*) from the National Technical University of Athens, Athens, Greece, and the M.S. and Ph.D. degrees in electrical engineering and computer science from The University of Michigan at Ann Arbor, Ann Arbor, MI, USA.

He is currently a Professor with the School of Electrical and Computer Engineering, Georgia Institute of Technology. He has authored or coauthored over 450 papers in refereed journals and conference proceedings, five books, and 19 book chapters. He has helped develop academic programs in highly integrated/multilayer packaging for RF and wireless applications using ceramic and organic flexible materials, paper-based RF identifications (RFIDs) and sensors, "green" electronics and power scavenging, nanotechnology applications in RF, microwave MEMs, system-on-package (SOP)-integrated (ultra-wideband (UWB), multiband, conformal) antennas, and adaptive numerical electromagnetics (finite difference time domain (FDTD), multiresolution algorithms) and heads the ATHENA research group (20 researchers). He has served as the Georgia Electronic Design Center Associate Director for RFID/Sensors research (2006–2010) and he has been the Georgia Institute of Technology National Science Foundation (NSF) Packaging Research Center Associate Director for RF Research and the RF Alliance Leader (2003–2006). In Summer 2002, he was a Visiting Professor with the Technical University of Munich, Munich, Germany. In Summer 2009, he was a Visiting Professor with GTRI-Ireland, Athlone, Ireland. In Summer 2010 and Summer 2012, he was a Visiting Professor with LAAS-CNRS, Toulouse, France. He is an Associate Editor for the *International Journal on Antennas and Propagation*. He has given over 100 invited talks to various universities and companies worldwide.

Prof. Tentzeris was the Technical Program Committee (TPC) chair for the IEEE Microwave Theory and Techniques Society (IEEE MTT-S) International Microwave Symposium (IMS) in 2008 and the chair of the 2005 IEEE CEM-TD Workshop. He is the vice-chair of the RF Technical Committee (TC16), IEEE

CPMT Society. He is the founder and chair of the RFID Technical Committee (TC24), IEEE MTT-S and the secretary/treasurer of the IEEE C-RFID. He is an associate editor for the IEEE TRANSACTIONS ON MICROWAVE THEORY AND TECHNIQUES and the IEEE TRANSACTIONS ON ADVANCED PACKAGING. He is a Member of URSI-Commission D and the MTT-15 Committee. He is an Associate Member of the European Microwave Association (EuMA). He is a Fellow of the Electromagnetic Academy. He is a Member of the Technical Chamber of Greece. He was an IEEE MTT-S Distinguished Microwave Lecturer (2010–2012). He was the recipient/corecipient of the 2012 Finland Distinguished Professor Award (Fi.Di.Pro.), the 2012 ICMG Architecture IT Excellence Award, the 2010 IEEE AP-S Piergiorgio L. E. Uslenghi Letters Prize Paper Award, the 2011 Best Student Paper Award of the International Workshop on Structural Health Monitoring, the 2010 Georgia Institute of Technology Senior Faculty Outstanding Undergraduate Research Mentor Award, the 2009 IEEE TRANSACTIONS ON COMPONENTS AND PACKAGING TECHNOLOGIES Best Paper Award, the 2009 E. T. S. Walton Award of the Irish Science Foundation, the 2007 IEEE AP-S Symposium Best Student Paper Award, the 2007 IEEE MTT-S IMS Third Best Student Paper Award, the 2007 ISAP 2007 Poster Presentation Award, the 2006 IEEE MTT-S Outstanding Young Engineer Award, the 2006 Asia–Pacific Microwave Conference Award, the 2004 IEEE TRANSACTIONS ON ADVANCED PACKAGING Commendable Paper Award, the 2003 NASA Godfrey "Art" Anzic Collaborative Distinguished Publication Award, the 2003 IBC International Educator of the Year Award, the 2003 IEEE CPMT Outstanding Young Engineer Award, the 2002 International Conference on Microwave and Millimeter-Wave Technology Best Paper Award, Beijing, China, the 2002 Georgia Institute of Technology Electrical and Computer Engineering Outstanding Junior Faculty Award, the 2001 ACES Conference Best Paper Award, the 2000 NSF CAREER Award, and the 1997 Best Paper Award of the International Hybrid Microelectronics and Packaging Society.